

Low-loss superconducting nanowire circuits using a neon focused ion beam

J. Burnett,^{1,*} J. Sagar,¹ O. W. Kennedy,¹ P. A. Warburton,¹ and J. C. Fenton^{1,†}

¹*London Centre for Nanotechnology, UCL, 17-19 Gordon Street, London, WC1H 0AH, UK*

(Dated: March 7, 2024)

We present low-temperature measurements of low-loss superconducting nanowire-embedded resonators in the low-power limit relevant for quantum circuits. The superconducting resonators are embedded with superconducting nanowires with widths down to 20 nm using a neon focused ion beam. In the low-power limit, we demonstrate an internal quality factor up to 3.9×10^5 at 300 mK (implying a TLS-limited quality factor up to 2×10^5 at 10 mK), not only significantly higher than in similar devices, but also matching the state of the art of conventional Josephson-junction-embedded resonators. We also show a high sensitivity of the nanowire to stray infrared photons, which is controllable by suitable precautions to minimise stray photons in the sample environment. Our results suggest that there are excellent prospects for superconducting-nanowire-based quantum circuits.

I. INTRODUCTION

Quantum circuits based on conventional Josephson-junctions have begun to tackle real-world problems¹. This has been despite high decoherence produced by the loss^{2,3} and noise^{4,5} caused by parasitic two-level systems (TLS)^{6,7}. In principle, superconducting nanowires can provide a route to low-decoherence quantum circuits due to their monolithic structure and lack of a TLS-hosting oxide layer. To date, superconducting nanowires with cross-sectional areas approaching the coherence length have demonstrated a variety of Josephson^{8,9} and phase-slip^{10–13} effects, but features such as their unconventional current-phase relationships¹⁴ remain unexploited in quantum circuits. Previous demonstrations of superconducting nanowire-embedded resonators exhibit unusually high dissipation, with internal quality factors (Q_i) below 5×10^3 ,^{10–12,15} far lower than in similar conventional Josephson-junction-based circuits^{16,17}. In general, the performance of nanowire-embedded resonators can be limited by material quality, interface imperfections, resist residues and the measurement environment.

We demonstrate superconducting nanowire-embedded circuits with single photon Q_i up to 3.9×10^5 , comparable to or even better than conventional Josephson-junction resonators. Superconducting nanowires with widths down to 20 nm were fabricated with a neon focused ion beam (FIB). We study the loss in our devices within the well-established framework of loss mechanisms in superconducting resonators^{2,3,7,18,19} to determine which factors are significant in limiting their performance. The vastly improved Q_i demonstrates that the detrimental effects can be sufficiently reduced and shows that competitive quantum circuits could be based on monolithic nanowire technology.

II. METHODS

Superconducting 20-nm-thick NbN films were deposited on sapphire by dc magnetron sputtering from a 99.99%-pure Nb target in a 1:1 Ar:N₂ atmosphere. The

vacuum chamber was pumped to 6×10^{-7} mbar before sputtering at a pressure of 3.5×10^{-3} mbar and power of 200 W. The superconducting critical temperature, T_c , was 10 K with a sheet resistance of $450 \Omega/sq$. Electron-beam lithography (EBL) was used to pattern $\lambda/4$ and $\lambda/2$ coplanar microwave resonators capacitively coupled to a common microwave feed line (shown in Fig. 1d). The width of the central conductor was $10 \mu m$ and the gap was $5 \mu m$. This pattern was transferred from a 300-nm-thick-layer of polymethyl methacrylate (PMMA) into the film by a reactive ion etch (RIE) using a 2:1 ratio of SF₆:Ar, at 30 W and 30 mbar.

A neon FIB was used to directly pattern²⁰ nanowires in the central conductor of the microwave resonators at the current antinode - see Fig. 1b. With an acceleration voltage of 15 kV, the clearance dose for the NbN film is $\approx 0.3 \text{ nC}/\mu m^2$. 15 kV was chosen as a compromise between minimising the spot size and minimising lateral milling of the nanowire²¹, leading to a few-minute mill time per μm^2 for a ~ 1 pA beam current. By prior patterning of a sub-200-nm-wide precursor wire in the same EBL step as the resonator (shown in Fig. 1c), we minimise the mill time and the total neon flux that the nanowire is subject to. Several devices were measured, and Table I shows important parameters including nanowire dimensions. The nanowire devices all feature two nanowires, configured either in parallel so that the nanowires complete a superconducting loop¹², or in series with a wider segment in between²². Here, there is no external flux- or gate-bias, so the nanowires are treated as simple constrictions within the superconductor.

Samples were enclosed within a brass box and cooled using a ³He refrigerator containing a heavily attenuated microwave in-line and an out-line with a cryogenic high-electron-mobility transistor (HEMT) amplifier.

III. RESULTS & DISCUSSION

Figure 1a shows the forward transmission (S_{21}) magnitude response of a nanowire-embedded resonator, at 307 mK and for an applied microwave drive of

−105 dBm, demonstrating $Q_i = 5.2 \times 10^5$. This Q_i is significantly higher than in comparable nanowire-based devices^{10–12,15}. This highlights the promise of the neon FIB and demonstrates that superconducting nanowires are not intrinsically lossy. The complex S_{21} notch response of the superconducting resonators is fitted by²³

$$S_{21}(\nu) = ae^{j\theta} e^{-2\pi j\nu\tau} \left[1 - \frac{(Q_L/|Q_c|)e^{j\phi}}{1 + 2jQ_L(\nu/\nu_0 - 1)} \right], \quad (1)$$

where ν is the applied frequency, ν_0 the resonance frequency, Q_L the loaded quality factor and $|Q_c|$ the absolute value of the coupling quality factor; ϕ accounts for impedance mismatches, a describes a change in amplitude, θ describes a change in phase and τ a change in the electronic delay. The internal quality factor, Q_i , is defined by $1/Q_L = 1/Q_i + \text{Re}(1/Q_c)$ and the energy within the resonator is $W_{\text{sto}} = 2P_{\text{app}}S_{\text{min}}Q_L/\omega_0$, where P_{app} is the applied microwave power (in W) and S_{min} the normalized minimum of the resonator magnitude response. We describe the microwave power in terms of the average number of photons in the resonator, $\langle n \rangle$, given by $\langle n \rangle = W_{\text{sto}}/(h\nu_0)$, where h is Planck's constant.

To examine the effect of the neon FIB on the NbN film, we measured the resonator response as a function of temperature (shown in Fig. 2). As temperature decreases from 2 K to 1 K, the resonant frequency increases due to changes in the complex conductivity which are described by $\frac{\Delta\nu}{\nu_0} = \frac{\alpha}{2} \frac{\Delta\sigma_2}{\sigma_2}$, where $\frac{\Delta\nu}{\nu_0}$ is the normalised resonance frequency, α is the kinetic inductance fraction and σ_2 is the imaginary part of the complex conductivity as given by Mattis-Bardeen (MB) theory²⁴. The inset of Fig. 2 shows the temperature dependence of the resonant frequency for all resonators on chip 1. The bunching of data points indicates a very similar T_c whether the resonator contains nanowires or not, implying that the neon FIB has not significantly suppressed the superconductivity.

Further decreasing temperature from 1 K, the resonant frequency decreases due to a thermal desaturation of TLS, which can be described by

$$\frac{\Delta\nu}{\nu_0} = \frac{F\delta_{\text{TLS}}^i}{\pi} \left[\text{Re}\Psi \left(\frac{1}{2} + \frac{1}{2\pi j} \frac{h\nu_0(T)}{k_B T} \right) - \ln \left(\frac{1}{2} \frac{h\nu_0(T_0)}{k_B T} \right) \right], \quad (2)$$

where F is the filling factor which typically relates to device geometry and electric field density, T_0 is a reference temperature, Ψ is the complex digamma function and $F\delta_{\text{TLS}}^i$ is the intrinsic loss tangent. Fig. 2 shows a fit to both the MB and TLS frequency shifts, and the extracted $F\delta_{\text{TLS}}^i$ is shown in Table I. Barends *et al.*²⁵ have previously showed that, to determine $F\delta_{\text{TLS}}^i$ using both MB and TLS models, it is not necessary to obtain data in the temperature range covering the frequency upturn below 100mK seen in the TLS fit curve in Fig. 2.

The thermal desaturation of TLS below 1 K results in absorption of microwave photons, leading to a power- and temperature-dependent resonator loss rate^{2,3}. At low microwave drive, the unsaturated TLS dominate the loss, but as the microwave drive increases these TLS become

saturated and therefore their loss rate decreases. At high microwave drives, where the TLS are saturated, the loss becomes dominated by residual quasiparticles, with a loss rate δ_{qp} which is temperature-dependent but assumed to be independent of microwave power¹⁹. The TLS and quasiparticle loss behaviour can be described by

$$\frac{1}{Q_i} = \delta_{\text{tot}}^i = F\delta_{\text{TLS}}^0 \frac{\tanh\left(\frac{h\nu_0}{2k_B T}\right)}{\left(1 + \left(\frac{\langle n \rangle}{n_c}\right)\right)^\beta} + \delta_{\text{qp}}, \quad (3)$$

where n_c is the number of photons equivalent to the saturation field of the TLS, β describes how quickly the TLS saturate with power and $F\delta_{\text{TLS}}^0$ is the TLS loss tangent ($F\delta_{\text{TLS}}^0$ is power- and temperature-independent). TLS models were originally based on the anomalous properties of glasses at low temperatures⁶ and assumed non-interacting TLS, which leads to a prediction of $\beta = 0.5$. However, as superconducting circuits have improved, this model has failed to accurately describe the power dependence of dielectric losses: a weaker power dependence with $\beta < 0.5$ is frequently found^{3,26–28}. This showed the need to consider TLS interactions^{4,5,7,26,29}, changing the loss model to^{7,29}

$$\frac{1}{Q_i} = FP_\gamma\chi \ln\left(\frac{Cn_c}{n} + \delta'_{\text{qp}}\right) \tanh\left(\frac{h\nu_0}{2k_B T}\right), \quad (4)$$

where χ is the dimensionless TLS parameter, P_γ is the TLS switching rate ratio, C is a large constant and δ'_{qp} is the log-scaled quasiparticle loss rate.

This loss is examined in more detail by fitting the resonator S_{21} response as a function of microwave drive and temperature (shown in Figs. 3a–c). Fig. 3a (Fig. 3c) show measurements of δ_{tot}^i (where $\delta_{\text{tot}}^i = 1/Q_i$) as a function of $\langle n \rangle$ on bare (nanowire-embedded) resonators. Each resonator has its own symbol, with solid (hollow) symbols corresponding to measurements in a normal (Eccosorb-lined) sample box. Eccosorb CR-117 (see supplemental³⁰) is a microwave absorber which has been shown to reduce quasiparticle excitation from stray infrared (IR) photons³¹, the Eccosorb lining is shown in Fig. 1e. Different colours correspond to different temperatures. When analysing Figs. 3a & c with Eq. 3, we find $\beta \approx 0.1–0.2$ (see supplemental³⁰) implying interacting TLS. The solid lines represent fits to the interacting-TLS model, Eq. 4. Table I collects fit parameters from both models.

We first consider bare resonators measured in a standard sample box (solid symbols in Fig. 3b). Resonators on the same chip show a fabrication-based variability, also found in the literature^{2,19,32}: high- $\langle n \rangle$ $Q_i = 1.2–3.1 \times 10^6$ and low- $\langle n \rangle$ $Q_i = 3.6–5.7 \times 10^5$ at 307 mK. Increasing the temperature leads to an increase in low- $\langle n \rangle$ Q_i because, as thermal occupation of the TLS increases, their ability to absorb microwave photons decreases^{3,32}, as described by the tanh temperature term. Increasing temperature also leads to a decrease in high- $\langle n \rangle$ Q_i . This is due to a higher quasiparticle density, meaning that more energy is lost to the quasiparticle system¹⁹.

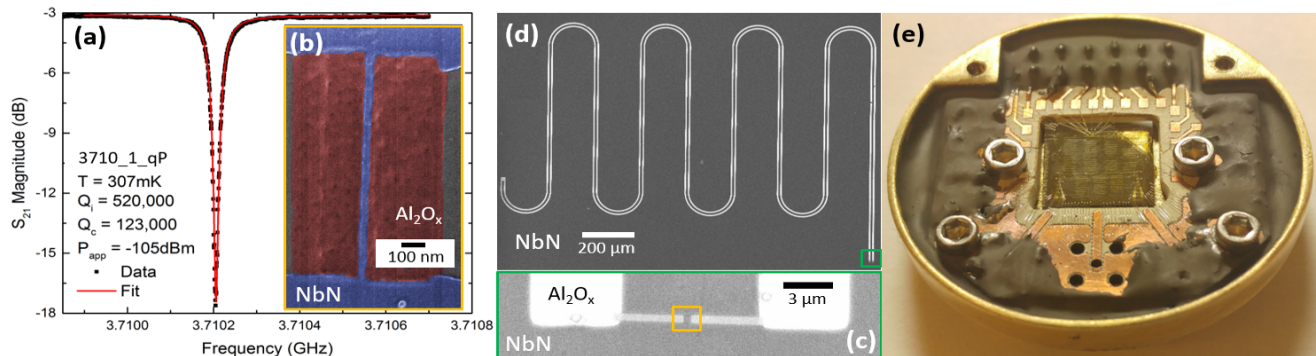


Figure 1. (a) The S_{21} magnitude response of the nanowire-embedded resonator 3710.1qP. The red line is a fit to Eq. 1. (b) A false-colour He FIB micrograph of a neon FIB milled nanowire (3710.1qP) with dimensions of 27 nm by 1.2 μm . The NbN is shown in blue, while the milled region is shown in red. (c, d) Scanning electron micrographs of (c) the shorted end of a $\lambda/4$ resonator before milling by neon FIB. (d) the whole $\lambda/4$ resonator. (e) A photograph of the sample holder. In the centre is a chip, which is wirebonded to a microwave printed circuit board, the dark material is Eccosorb.

Table I. Table of resonator parameters. Resonators are named by ν_0 (MHz), their chip number, $\lambda/4$ (q) or $\lambda/2$ (h) and whether they are bare resonators (B), have nanowires in series (S), have nanowires in parallel (P) or were measured in an Eccosorb-lined box (E). \bar{w} refers to the nanowire widths. δ_{TLS}^i comes from fits to Eq. 2, while δ_{TLS}^0 & δ_{qp} come from fits to Eq. 3 and $FP\gamma\chi$ come from fits to Eq. 4.

Resonator	\bar{w} (nm)	$F\delta_{\text{TLS}}^i$ ($\times 10^{-6}$)	$FP\gamma\chi$ ($\times 10^{-6}$)	$F\delta_{\text{TLS}}^0$ ($\times 10^{-6}$)	δ_{qp} ($\times 10^{-7}$)
4094_1qB	-	6	0.57	6.6	5.6
3995_1hB	-	6.3	0.61	6.2	6.9
3675_2qBE	-	9.8	1.11	9.5	5.6
2739_2hBE	-	12.6	1.21	10.2	13.3
3710_1qP	27, 30	4.8	0.47	5.9	12.4
3012_1hS	47, 48	6.9	0.42	7.8	21.1
3382_2qPE	20, 23	12.9	1.13	14.3	5.4
3468_2hSE	37, 34	13.0	1.27	14.2	6.8

We next consider nanowire-embedded resonators in the standard sample box (solid symbols in Fig. 3c). At 307 mK, at low $\langle n \rangle$, we find $Q_i = 2.7\text{--}3.9 \times 10^5$, in good agreement with the results from the bare resonators, so the FIB-based fabrication of the nanowire has produced very little additional TLS loss. At high $\langle n \rangle$, we find $Q_i = 4.1\text{--}7.2 \times 10^5$, 3–5 times lower than the bare resonators, indicating a higher residual quasiparticle density for the nanowire-embedded resonators.

Quasiparticles generated from pair-breaking events are an important consideration in conventional Josephson-junction devices³³, where Eccosorb is typically used to reduce quasiparticle-based losses caused by stray IR photons^{31,33}. We examined whether quasiparticles generated from IR photons are important for nanowire-embedded resonators by measuring them in an Eccosorb-lined sample box. As the hollow dotted symbols in Fig. 3c show, losses at high $\langle n \rangle$ are much lower than for the standard sample box and $Q_i \approx 6\text{--}9 \times 10^5$. This value matches

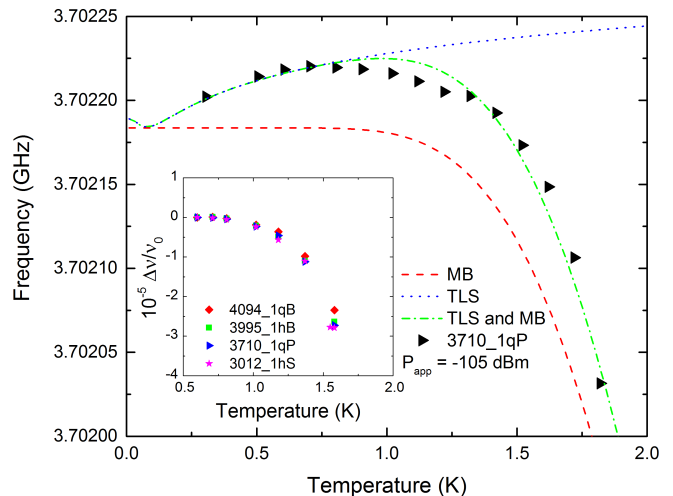


Figure 2. Resonant frequency of resonator 3710.1qP as a function of temperature. Red broken line: Variation arising from kinetic inductance changes described by MB theory. Blue dotted line: Variation arising from TLS losses. Green dash-dotted line: Fit to data including both MB and TLS effects. Inset: Normalised frequency shift as a function of temperature for all resonators on chip 1.

that of the bare resonators for the same $\langle n \rangle$, suggesting that the density of residual quasiparticles has been reduced to that of the bare resonators (see Table I). A saturated high- $\langle n \rangle$ Q_i is not observed, due to nonlinearities in the resonance lineshape of the nanowire-embedded resonators. With the smaller quasiparticle-based loss, the TLS-based low- $\langle n \rangle$ trend of loss increasing as $\langle n \rangle$ decreases is once again found. The high- $\langle n \rangle$ Q_i is found to increase with increasing temperature, consistent with losses from thermally generated quasiparticles as found in the bare resonators, indicating that increased quasiparticle losses in nanowire-embedded resonators in the normal sample box arose from quasiparticles excited by IR pho-

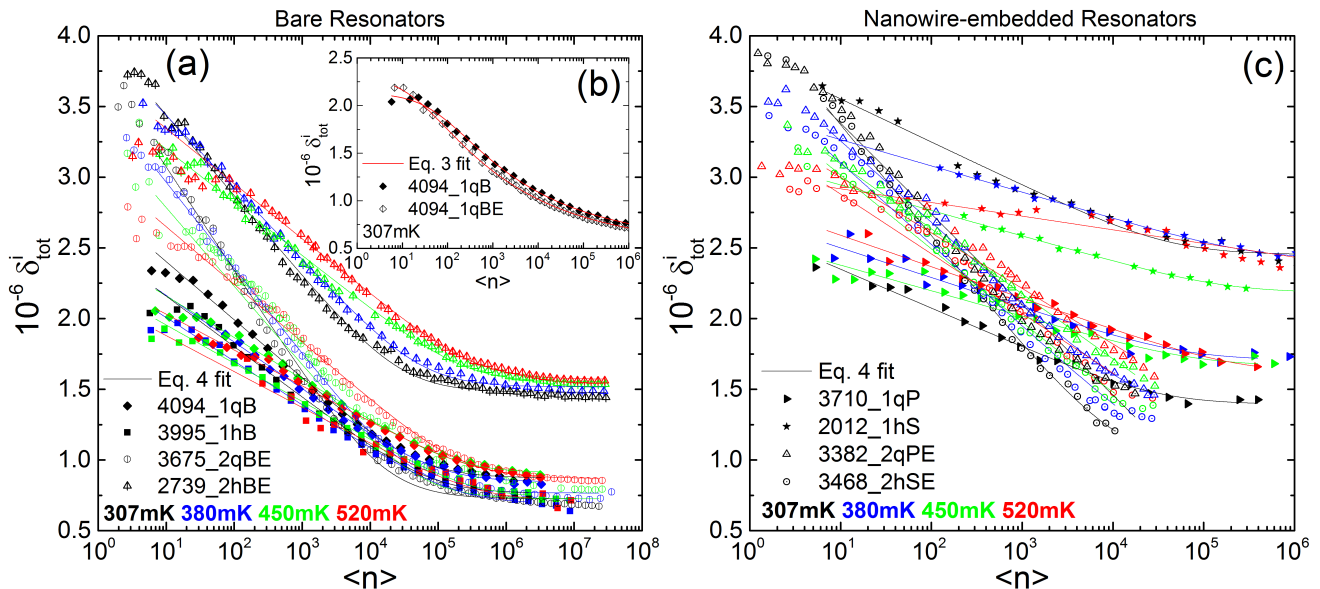


Figure 3. (a) Loss tangent ($\delta_{\text{tot}}^i = 1/Q_i$) as a function of microwave drive for bare resonators. The colours correspond to different temperatures and the hollow symbols indicate the use of an Eccosorb CR-117 lined sample box. The solid lines in all plots represent fits to Eq. 4. (b) Loss tangent for the resonator 4094_1qB with and without the Eccosorb-lined box. (c) Loss tangent as a function of microwave drive for the nanowire-embedded resonators.

tons. As Table I shows, δ_{qp} of the nanowire-embedded resonators in the Eccosorb environment match those of the bare resonators (both with and without the Eccosorb environment) and are therefore limited by another mechanism which is not unique to the nanowire.

Figure 3b shows the loss for the same bare resonator with and without the Eccosorb enclosure. In contrast to nanowire-embedded resonators, the high- $\langle n \rangle$ loss decreases only slightly when the Eccosorb-lined sample box is used. This is actually unsurprising since the energy gap of NbN is $\sim 10\times$ larger than in Al. On the other hand, the reason for the sensitivity to IR photons in the nanowire-embedded resonators is not immediately obvious. Our results demonstrate the importance of IR filtering even when nanowires have a large superconducting energy gap such as those in NbN. This is relevant to all nanowire-based devices. We note that a small suppression of T_c in our nanowire (below the precision of our T_c determination) could give some enhanced sensitivity to IR photons. Alternative explanations for the sensitivity include the nanowire exhibiting a different quasiparticle lifetime³⁴ or non-equilibrium superconductivity³⁵, but these are beyond the scope of this study, although, since Q_i remains high, the number of quasiparticles created from IR photons must still be quite small³¹.

Finally, we compare the consistency of the TLS-loss rates (Table I and supplemental³⁰) obtained from the analysis of the data shown in Figs. 2 & 3. $F\delta_{\text{TLS}}^i$ and $F\delta_{\text{TLS}}^0$ differ by less than 20%, this difference is because $F\delta_{\text{TLS}}^0$ is only sensitive to near-resonant TLS, whereas $F\delta_{\text{TLS}}^i$ is also sensitive to a broad spectrum of off-resonant TLS^{3,32,36}. Next, we note that $\delta_{\text{TLS}}^i = \chi$,⁷

so that the ratio $FP_\gamma\chi/F\delta_{\text{TLS}}^i$ gives P_γ . We find an average value of $P_\gamma = 0.093$. This agrees well (see supplemental³⁰) with the charge noise spectra of single-electron transistors that give $P_\gamma \approx 0.10$.^{37,38} Therefore, all TLS-loss rates are consistent with each other. The TLS loss rates imply a TLS-limited Q_i up to $\approx 2\times 10^5$ in the quantum limit (at temperatures down to 10 mK and at single-photon energies). This is approximately $100\times$ larger than in equivalent nanowire-embedded resonators and compares favourably with Josephson-junction-embedded resonators.

IV. CONCLUSION

To conclude, we have used a neon FIB to create superconducting nanowires with widths down to 20 nm within superconducting resonators. In the low-power limit, these devices demonstrated Q_i up to 3.9×10^5 at 300 mK, with δ_{TLS}^i and δ_{TLS}^0 corresponding to a TLS-limited Q_i up to 2×10^5 at 10 mK. These TLS losses arise from the NbN thin-film technology rather than the neon FIB, meaning a higher Q_i should be possible with better resonator technology³². By obtaining such a high Q_i using nanowires, we have demonstrated a critical step towards realising nanowire-based, superinductance, phase-slip or Dayem-bridge circuits with coherence times comparable to conventional Josephson-junction-type devices.

V. ACKNOWLEDGEMENTS

The authors would like to acknowledge useful discussions with S. de Graaf, E. Dupont-Ferrier, N. Constantino and T. Lindström. We also thank T. Lindström

for the loan of equipment and critical reading of the manuscript. The authors gratefully acknowledge funding from the UK EPSRC, grant references EP/J017329/1 (JB and JCF) and EP/K024701/1 (JS and PAW), and Carl Zeiss SMT (JS and PAW).

-
- * burnett@chalmers.se
 † j.fenton@ucl.ac.uk
- ¹ P. J. J. O'Malley, R. Babbush, I. D. Kivlichan, J. Romero, J. R. McClean, R. Barends, J. Kelly, P. Roushan, A. Tranter, N. Ding, B. Campbell, Y. Chen, Z. Chen, B. Chiaro, A. Dunsworth, A. G. Fowler, E. Jeffrey, E. Lucero, A. Megrant, J. Y. Mutus, M. Neeley, C. Neill, C. Quintana, D. Sank, A. Vainsencher, J. Wenner, T. C. White, P. V. Coveney, P. J. Love, H. Neven, A. Aspuru-Guzik, and J. M. Martinis, Scalable quantum simulation of molecular energies, *Phys. Rev. X* **6**, 031007 (2016).
 - ² T. Lindström, J. E. Healey, M. S. Colclough, C. M. Muirhead, and A. Ya. Tzalenchuk, Properties of superconducting planar resonators at millikelvin temperatures, *Phys. Rev. B* **80**, 132501 (2009).
 - ³ P. Macha, S. H. W. van der Ploeg, G. Oelsner, E. Ilichev, H.-G. Meyer, S. Wnsch, and M. Siegel, Losses in coplanar waveguide resonators at millikelvin temperatures, *Applied Physics Letters* **96**, 062503 (2010).
 - ⁴ J Burnett, L Faoro, I Wisby, V L Gurtovoi, A V Chernykh, G M Mikhailov, V A Tulin, R Shaikhaidarov, V Antonov, PJ Meeson, A Ya Tzalenchuk, and T Lindström, Evidence for interacting two-level systems from the $1/f$ noise of a superconducting resonator, *Nature Communications* **5**, 4119 (2014).
 - ⁵ AN Ramanayaka, B Sarabi, and KD Osborn, Evidence for universal relationship between the measured $1/f$ permittivity noise and loss tangent created by tunneling atoms, arXiv preprint arXiv:1507.06043 (2015).
 - ⁶ WA Phillips, Tunneling states in amorphous solids, *Journal of Low Temperature Physics* **7**, 351–360 (1972).
 - ⁷ Lara Faoro and Lev B. Ioffe, Interacting tunneling model for two-level systems in amorphous materials and its predictions for their dephasing and noise in superconducting microresonators, *Phys. Rev. B* **91**, 014201 (2015).
 - ⁸ L Hao, D C Cox, and J C Gallop, Characteristics of focused ion beam nanoscale josephson devices, *Superconductor Science and Technology* **22**, 064011 (2009).
 - ⁹ E. M. Levenson-Falk, R. Vijay, and I. Siddiqi, Nonlinear microwave response of aluminum weak-link josephson oscillators, *Applied Physics Letters* **98**, 123115 (2011).
 - ¹⁰ OV Astafiev, LB Ioffe, S Kafanov, Yu A Pashkin, K Yu Arutyunov, D Shahar, O Cohen, and JS Tsai, Coherent quantum phase slip, *Nature* **484**, 355–358 (2012).
 - ¹¹ J. T. Peltonen, Z. H. Peng, Yu. P. Korneeva, B. M. Voronov, A. A. Korneev, A. V. Semenov, G. N. Gol'tsman, J. S. Tsai, and O. V. Astafiev, Coherent dynamics and decoherence in a superconducting weak link, *Phys. Rev. B* **94**, 180508 (2016).
 - ¹² Andrey Belkin, Matthew Brenner, Thomas Aref, Jaseung Ku, and Alexey Bezryadin, Littleparks oscillations at low temperatures: Gigahertz resonator method, *Applied Physics Letters* **98**, 242504 (2011).
 - ¹³ C. H. Webster, J. C. Fenton, T. T. Hongisto, S. P. Giblin, A. B. Zorin, and P. A. Warburton, Nbsi nanowire quantum phase-slip circuits: dc supercurrent blockade, microwave measurements, and thermal analysis, *Phys. Rev. B* **87**, 144510 (2013).
 - ¹⁴ KK Likharev, Superconducting weak links, *Reviews of Modern Physics* **51**, 101 (1979).
 - ¹⁵ Mark David Jenkins, Uta Naether, Miguel Ciria, Javier Ses, James Atkinson, Carlos Snchez-Azqueta, Enrique del Barco, Johannes Majer, David Zueco, and Fernando Luis, Nanoscale constrictions in superconducting coplanar waveguide resonators, *Applied Physics Letters* **105**, 162601 (2014).
 - ¹⁶ S. E. de Graaf, J. Leppäkangas, A. Adamyan, A. V. Danilov, T. Lindström, M. Fogelström, T. Bauch, G. Johansson, and S. E. Kubatkin, Charge qubit coupled to an intense microwave electromagnetic field in a superconducting nb device: Evidence for photon-assisted quasiparticle tunneling, *Phys. Rev. Lett.* **111**, 137002 (2013).
 - ¹⁷ M. Simoen, C. W. S. Chang, P. Krantz, Jonas Bylander, W. Wustmann, V. Shumeiko, P. Delsing, and C. M. Wilson, Characterization of a multimode coplanar waveguide parametric amplifier, *Journal of Applied Physics* **118**, 154501 (2015).
 - ¹⁸ C. M. Quintana, A. Megrant, Z. Chen, A. Dunsworth, B. Chiaro, R. Barends, B. Campbell, Yu Chen, I.-C. Hoi, E. Jeffrey, J. Kelly, J. Y. Mutus, P. J. J. O'Malley, C. Neill, P. Roushan, D. Sank, A. Vainsencher, J. Wenner, T. C. White, A. N. Cleland, and John M. Martinis, Characterization and reduction of microfabrication-induced decoherence in superconducting quantum circuits, *Applied Physics Letters* **105**, 062601 (2014).
 - ¹⁹ Jan Goetz, Frank Deppe, Max Haerberlein, Friedrich Wulschner, Christoph W. Zollitsch, Sebastian Meier, Michael Fischer, Peter Eder, Edwar Xie, Kirill G. Fedorov, Edwin P. Menzel, Achim Marx, and Rudolf Gross, Loss mechanisms in superconducting thin film microwave resonators, *Journal of Applied Physics* **119**, 015304 (2016).
 - ²⁰ R Timilsina, S Tan, R Livengood, and P D Rack, Monte carlo simulations of nanoscale focused neon ion beam sputtering of copper: elucidating resolution limits and subsurface damage, *Nanotechnology* **25**, 485704 (2014).
 - ²¹ F. H. M. Rahman, Shawn McVey, Louis Farkas, John A. Notte, Shida Tan, and Richard H. Livengood, The prospects of a subnanometer focused neon ion beam, *Scanning* **34**, 129–134 (2012).
 - ²² T. T. Hongisto and A. B. Zorin, Single-charge transistor based on the charge-phase duality of a superconducting nanowire circuit, *Phys. Rev. Lett.* **108**, 097001 (2012).
 - ²³ S. Probst, F. B. Song, P. A. Bushev, A. V. Ustinov, and M. Weides, Efficient and robust analysis of complex scattering data under noise in microwave resonators, *Review of Scientific Instruments* **86**, 024706 (2015).

- ²⁴ DC Mattis and John Bardeen, Theory of the anomalous skin effect in normal and superconducting metals, *Physical Review* **111**, 412 (1958).
- ²⁵ R Barends, HL Hortensius, Tony Zijlstra, Jochem JA Baselmans, SJC Yates, JR Gao, and Teun M Klapwijk, Noise in nbtin, al, and ta superconducting resonators on silicon and sapphire substrates, *IEEE Transactions on Applied Superconductivity* **19**, 936–939 (2009).
- ²⁶ J Burnett, L Faoro, and T Lindström, Analysis of high quality superconducting resonators: consequences for tls properties in amorphous oxides, *Superconductor Science and Technology* **29**, 044008 (2016).
- ²⁷ David S. Wisbey, Jiansong Gao, Michael R. Vissers, Fabio C. S. da Silva, Jeffrey S. Kline, Leila Vale, and David P. Pappas, Effect of metal/substrate interfaces on radio-frequency loss in superconducting coplanar waveguides, *Journal of Applied Physics* **108**, 093918 (2010).
- ²⁸ M. S. Khalil, F. C. Wellstood, and K. D. Osborn, Loss dependence on geometry and applied power in superconducting coplanar resonators, *IEEE Transactions on Applied Superconductivity* **21**, 879–882 (2011).
- ²⁹ Lara Faoro and Lev B. Ioffe, Internal loss of superconducting resonators induced by interacting two-level systems, *Phys. Rev. Lett.* **109**, 157005 (2012).
- ³⁰ See Supplemental Material at [URL will be inserted by publisher] for details of the experimental setup & further discussion of TLS losses.
- ³¹ R. Barends, J. Wenner, M. Lenander, Y. Chen, R. C. Bialczak, J. Kelly, E. Lucero, P. O'Malley, M. Mariantoni, D. Sank, H. Wang, T. C. White, Y. Yin, J. Zhao, A. N. Cleland, John M. Martinis, and J. J. A. Baselmans, Minimizing quasiparticle generation from stray infrared light in superconducting quantum circuits, *Applied Physics Letters* **99**, 113507 (2011).
- ³² A. Bruno, G. de Lange, S. Asaad, K. L. van der Enden, N. K. Langford, and L. DiCarlo, Reducing intrinsic loss in superconducting resonators by surface treatment and deep etching of silicon substrates, *Applied Physics Letters* **106**, 182601 (2015).
- ³³ Antonio D. Crcoles, Jerry M. Chow, Jay M. Gambetta, Chad Rigetti, J. R. Rozen, George A. Keefe, Mary Beth Rothwell, Mark B. Ketchen, and M. Steffen, Protecting superconducting qubits from radiation, *Applied Physics Letters* **99**, 181906 (2011).
- ³⁴ P. J. de Visser, J. J. A. Baselmans, P. Diener, S. J. C. Yates, A. Endo, and T. M. Klapwijk, Number fluctuations of sparse quasiparticles in a superconductor, *Phys. Rev. Lett.* **106**, 167004 (2011).
- ³⁵ D J Goldie and S Withington, Non-equilibrium superconductivity in quantum-sensing superconducting resonators, *Superconductor Science and Technology* **26**, 015004 (2013).
- ³⁶ D. P. Pappas, M. R. Vissers, D. S. Wisbey, J. S. Kline, and J. Gao, Two level system loss in superconducting microwave resonators, *IEEE Transactions on Applied Superconductivity* **21**, 871–874 (2011).
- ³⁷ S. Kafanov, H. Brenning, T. Duty, and P. Delsing, Charge noise in single-electron transistors and charge qubits may be caused by metallic grains, *Phys. Rev. B* **78**, 125411 (2008).
- ³⁸ This arises from $P_\gamma = 1/\ln(\gamma_{\max}/\gamma_{\min})$, where γ_{\max} (γ_{\min}) is the maximum (minimum) rate of TLS switching. For a TLS charge noise spectrum extending from a few Hz to a few 100kHz, $P_\gamma \approx 0.1$.
- ³⁹ D F Santavicca and D E Prober, Impedance-matched low-pass stripline filters, *Measurement Science and Technology* **19**, 087001 (2008).
- ⁴⁰ Simon Gustavsson, Fei Yan, Gianluigi Catelani, Jonas Bylander, Archana Kamal, Jeffrey Birenbaum, David Hover, Danna Rosenberg, Gabriel Samach, Adam P. Sears, Steven J. Weber, Jonilyn L. Yoder, John Clarke, Andrew J. Kerman, Fumiki Yoshihara, Yasunobu Nakamura, Terry P. Orlando, and William D. Oliver, Suppressing relaxation in superconducting qubits by quasiparticle pumping, *Science* (2016).
- ⁴¹ RP Budoyo, JB Hertzberg, CJ Ballard, KD Voigt, Z Kim, JR Anderson, CJ Lobb, and FC Wellstood, Effects of nonequilibrium quasiparticles in a thin-film superconducting microwave resonator under optical illumination, *Physical Review B* **93**, 024514 (2016).
- ⁴² Jürgen Lisenfeld, Grigoriy J Grabovskij, Clemens Müller, Jared H Cole, Georg Weiss, and Alexey V Ustinov, Observation of directly interacting coherent two-level systems in an amorphous material, *Nature Communications* **6** (2015).
- ⁴³ S. T. Skacel, Ch. Kaiser, S. Wuensch, H. Rotzinger, A. Lukashenko, M. Jerger, G. Weiss, M. Siegel, and A. V. Ustinov, Probing the density of states of two-level tunneling systems in silicon oxide films using superconducting lumped element resonators, *Applied Physics Letters* **106**, 022603 (2015).
- ⁴⁴ Alexej Semenov, Burghardt Günther, Ute Böttger, H-W Hübers, Holger Bartolf, Andreas Engel, Andreas Schilling, Konstantin Ilin, Michael Siegel, R Schneider, D Gerthsen, and N A Gippius, Optical and transport properties of ultrathin nbn films and nanostructures, *Physical Review B* **80**, 054510 (2009).
- ⁴⁵ Pieter Cornelis Jenze Jan Coumou, *Electrodynamics of strongly disordered superconductors*, *PhD thesis* (TU Delft, Delft University of Technology, 2015).
- ⁴⁶ PJ De Visser, DJ Goldie, P Diener, S Withington, JJA Baselmans, and TM Klapwijk, Evidence of a nonequilibrium distribution of quasiparticles in the microwave response of a superconducting aluminum resonator, *Physical Review Letters* **112**, 047004 (2014).
- ⁴⁷ A. A. Adamyanyan, S. E. Kubatkin, and A. V. Danilov, Tunable superconducting microstrip resonators, *Applied Physics Letters* **108**, 172601 (2016).